Polaro–cryptic mirror of the lookdown as a biological model for open ocean camouflage

Parrish C. Brady[a,1], Kort A. Travis[a], Tara Maginnis[b], and Molly E. Cummings[a]

[a]Section of Integrative Biology, University of Texas at Austin, Austin, TX 78712; and [b]Department of Biology, University of Portland, Portland, OR 97203

Edited by Joanna Aizenberg, Harvard University, Cambridge, MA, and accepted by the Editorial Board May 2, 2013 (received for review December 19, 2012)

With no object to hide behind in 3D space, the open ocean represents a challenging environment for camouflage. Conventional strategies for reflective crypsis (e.g., standard mirror) are effective against axially symmetric radiance fields associated with high solar altitudes, yet ineffective against asymmetric polarized radiance fields associated with low solar inclinations. Here we identify a biological model for polaro–crypsis. We measured the surface-reflectance Mueller matrix of live open ocean fish (lookdown, *Selene vomer*) and seagrass-dwelling fish (pinfish, *Lagodon rhomboides*) using polarization-imaging and modeling polarization camouflage for the open ocean. Lookdowns occupy the minimization basin of our polarization-contrast space, while pinfish and standard mirror measurements exhibit higher contrast values than optimal. The lookdown reflective strategy achieves significant gains in polaro–crypsis (up to 80%) in comparison with nonpolarization sensitive strategies, such as a vertical mirror. Lookdowns achieve polaro–crypsis across solar altitudes by varying reflective properties (described by 16 Mueller matrix elements m_{ij}) with incident illumination. Lookdowns preserve reflected polarization aligned with principle axes (dorsal–ventral and anterior–posterior, $m_{22} = 0.64$), while randomizing incident polarization 45° from principle axes ($m_{33} = -0.05$). These reflectance properties allow lookdowns to reflect the uniform degree and angle of polarization associated with high-noon conditions due to alignment of the principle axes and the sun, and reflect a more complex polarization pattern at asymmetrical light fields associated with lower solar elevations. Our results suggest that polaro–cryptic strategies vary by habitat, and require context-specific depolarization and angle alteration for effective concealment in the complex open ocean environment.

The open ocean is the predominant habitat on earth with an abundance of predators and prey, yet with few other objects within it. Concealment strategies are therefore constrained to blend into the water medium itself (1, 2). Previous researchers recognized that the scattering environment of the water medium in the open ocean provides a largely axially symmetric radiance field within which a mirror held vertically would reflect the same light that it conceals (3). The reflective surfaces of some silvery fish are consistent with this vertical mirror strategy (4, 5). However, this same scattering environment also produces significant asymmetry in the polarized light fields (6, 7). Given the prevalence of polarization-sensitive vision in marine organisms (8–12), concealment strategies that account for this axial asymmetry are likely to exist, yet to date no quantitative evaluation of polarization camouflage (polaro–crypsis) has been conducted for a living organism.

Polaro–crypsis is challenging because the polarized light fields in the near-surface regions of the ocean vary with solar inclination angle (13), resulting in a polarization background that continually changes throughout the day (Fig. 1). In full sunlight, the degree of polarization (DoP) is maximal at an angle perpendicular, and minimal in parallel, to the sunlight propagation axis or solar ray (SR) (Fig. 1*A*) (14). This means that at high solar elevation conditions, an observer will experience high DoP in every azimuth direction, but as solar elevation decreases, the background will oscillate between high and low DoP depending on the azimuth viewing angle (Fig. 1 *A*, *C*, and *E*). Meanwhile, the angle of polarization (AoP) varies as a more complex relationship between the viewer and the main plane of polarization (plane perpendicular to the sunlight's propagation axis). Specifically, the background AoP is a function of the angle between the main plane of polarization and the viewing plane. When the two are in parallel (e.g., high noon), then the AoP will be uniformly horizontal (0°) (Fig. 1 *B* and *D*) in every azimuthal direction. However, as this angle increases, the AoP associated with viewing angles perpendicular to the solar plane will vary proportionately, while azimuth angles in line with the solar plane will retain a background AoP of 0° (Fig. 1 *B*, *D*, and *F*). Hence, unless the solar incident axis is directly overhead, the polarization background will be nonuniform and the AoP and DoP of this background will change depending on the azimuthal viewing direction, ψ (Fig. 1 *A*–*F*). For this reason, any animal attempting camouflage in this environment must manipulate its polarized reflectance in a directionally specific manner.

When the sun is directly overhead (solar inclination, $\theta_s = 90°$), a vertical mirror reflectance strategy (3) exhibits perfect polaro–crypsis (Fig. 1*G*, Movie S1) due to axial symmetry. Here the incoming Stokes vector equals the Stokes vector reflected off the organism (15). However, at lower solar inclination angles, a vertical mirror strategy is not ideal because background polarization becomes axially asymmetric, varying cyclically about the 360° azimuth (16) (Fig. 1*H*, Movie S1), and the reflected light will have polarization properties that are out of phase with the background. Hence, under these conditions, an optimal polaro–cryptic reflector would not behave as a vertical mirror, but rather as a surface that exhibits the capacity to both preserve and modify selected components of the incident polarization to blend into the background when observed from different viewing angles.

Here we evaluate whether fish have adopted a vertical mirror or some other polaro–cryptic strategy, by combining video polarimetery (17, 18) and polarization microscopy reflectance measurements of live open ocean fish, the lookdown (*Selene vomer*) and the seagrass-dwelling nearshore pinfish (*Lagodon rhomboides*), across a range of different incident polarization angles. From these measurements, we calculate the complete polarization characteristics of these organisms in the form of a Mueller matrix and identify the ideal contrast-minimizing properties of this matrix for open ocean conditions using optimality–parameter modeling. The Mueller matrix is the quantifiable physical characteristic of reflection that specifies how the incident Stokes vector is transformed into the reflected Stokes vector. The Stokes vector is a mathematical description of the polarized state with components of I (intensity), Q (principle axes of polarization), U (45° offset of the principle axes), and V (the elliptical measure of

Author contributions: P.C.B., T.M., and M.E.C. designed research; P.C.B., T.M., and M.E.C. performed research; P.C.B. contributed new reagents/analytic tools; P.C.B. and M.E.C. analyzed data; and P.C.B., K.A.T., and M.E.C. wrote the paper.

The authors declare no conflict of interest.

This article is a PNAS Direct Submission. J.A. is a guest editor invited by the Editorial Board.

[1]To whom correspondence may be addressed. E-mail: pbrady@physics.utexas.edu.

This article contains supporting information online at www.pnas.org/lookup/suppl/doi:10.1073/pnas.1222125110/-/DCSupplemental.

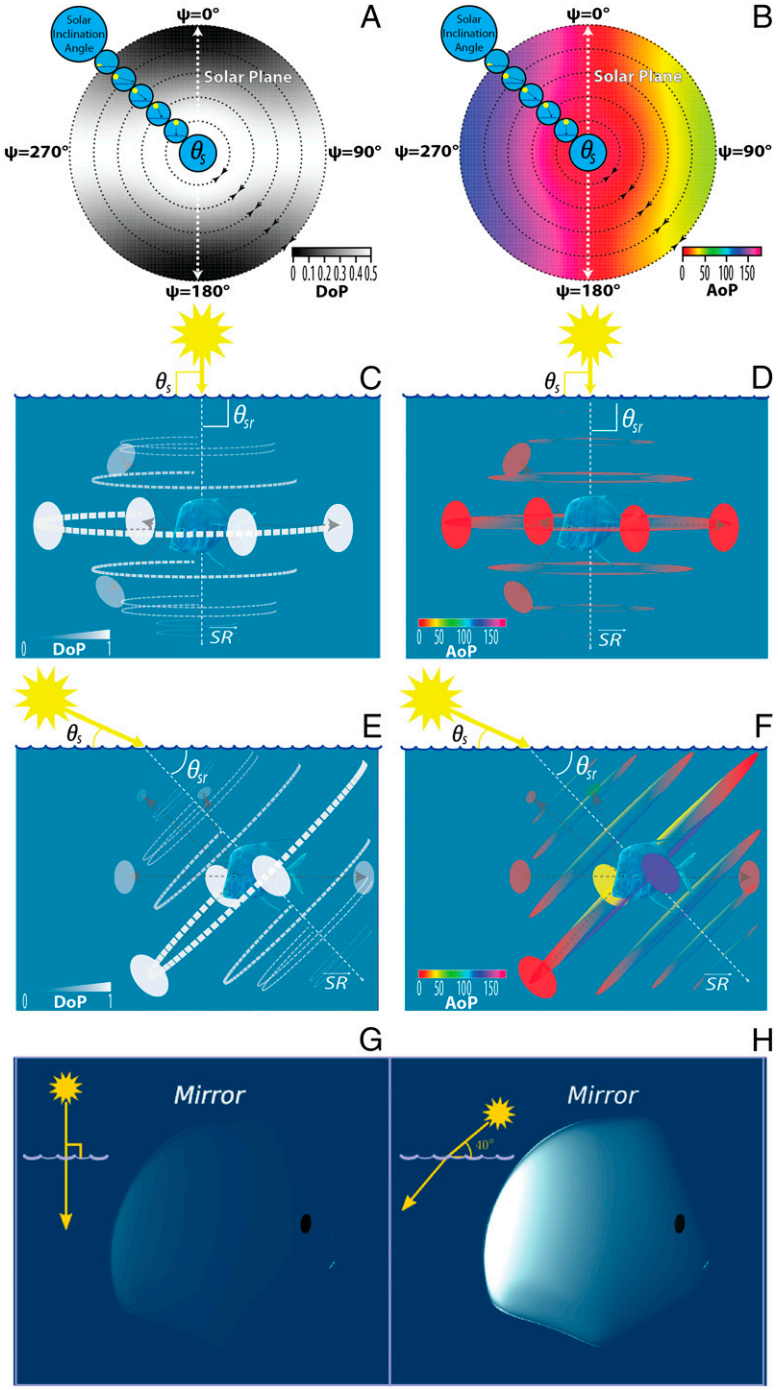

Fig. 1. Complexity of underwater polarization fields in relation to camouflage. Panels *A–F* describe and illustrate underwater polarization fields. In panels *A* and *B* the DoP and AoP values horizontally viewed are represented as a polar plot where the different radii of each concentric circle represent DoP (*A*) and AoP (*B*) associated with changes in θ_s, the above water solar inclination angle (represented in blue), and ψ, the azimuthal viewing angle (e.g., predator viewing angle) in relation to the solar plane. Panels *C–F* represent the 3D viewing environment in high solar inclination angle environments (*C* and *D*) and low solar inclination angle environments (*E* and *F*). θ_{sr} is the refracted solar angle in the water, and SR is the SR propagation direction. The dashed (*C* and *E*) or colored (*D* and *F*) planes perpendicular to SR represent the DoP (*C* and *E*) and AoP (*D* and *F*). The gray-scale (*C* and *E*) or colored (*D* and *F*) disks represent the visual DoP and AoP background properties in different viewing directions from the fish's frame of reference. Concentric ring radii and disk orientation and size are arbitrary. The last two panels (*G* and *H*) are 3D renderings of a fish body using the vertical mirror strategy at $\theta_s \sim 90°$ and $\theta_s \sim 40°$. For the rendering, the overall reflectance is scaled using the calculated Stokes contrast, with 10% diffuse reflectance added to allow the object to be visible in all cases (Movie S1).

polarized light). Principle axes usually correspond to the horizontal and vertical components of polarization with respect to the viewer's frame of reference, and for our purposes will be aligned with the plane parallel and perpendicular to the water surface when describing open ocean polarization fields or the anterior–posterior and dorsal–ventral axes of the fish. By varying the properties of specific Mueller matrix elements (m_{ij}) to identify the ideal polaro–cryptic strategy in the open ocean, we then compare idealized to realized polaro–cryptic performances of lookdowns, pinfish, and mirrors.

Results and Discussion

Neither lookdowns nor pinfish exhibited differences in reflectance intensities between illumination conditions (0° and 45° incident AoP) to the horizontal plane of the fish (lookdown $P = 0.11$; pinfish $P = 0.65$), with both species reflecting as much light as the polarization standard reflector (Fig. 2 *A* and *B*). However, there were distinct species-specific differences in AoP and DoP reflectance properties. As the AoP of the incident illumination changed from 0° to 45°, pinfish AoP reflectance changed with incident illumination (within ~1° of the standard in both conditions) (Fig. 2 *A* and *B*) and exhibited no difference in DoP reflectance between conditions (mean ± SD pinfish DoP with 0° AoP incident illumination = 0.34 ± 0.13 and 45° AoP incident illumination = 0.31 ± 0.14, $t_{44} = 0.89$, $P = 0.38$). In contrast to the pinfish, lookdowns exhibited a significant decrease in DoP when illuminated with an incident AoP of 45° relative to an incident AoP of 0° (Fig. 2 *A* and *B*) ($t_{46} = 5.63$, $P = 0.000006$) and reflected a significant difference in AoP reflectance from incident illumination of 45° AoP (Fig. 2 *A* and *B*) ($t_{44} = 19.08$, $P = 6.55 \times 10^{-23}$). Direct comparisons of the lookdown AoP reflectances in the two conditions confirm a similar near-horizontal (0° AoP) reflectance (mean ± SD lookdown AoP reflectance in 0° AoP incident illumination = 10.97° ± 4.68° and 45° AoP incident illumination = 10.0° ± 12.1°, $t_{44} = 0.37$, $P = 0.71$).

These results reveal that lookdowns reflect intensities similar to a composite quasi-specular broadband reflector, but vary polarized reflectance in a context-specific manner (Fig. 2 *A* and *B*). When lookdowns and pinfish are illuminated with homogenous polarization conditions associated with high solar inclinations (Fig. 1 *C* and *D*), both species exhibit similar reflectance in terms of intensity, DoP, and AoP (0° incident AoP conditions) (Fig. 2*B*). However, when illuminated with more complex polarization light fields associated with lower solar inclinations (Fig. 1 *E* and *F*), only the lookdown exhibits an ability to reflect polarized light with different AoP and DoP properties than the incident illumination (45° incident AoP conditions) (Fig. 2*B*). To determine the adaptiveness of such polarization reflectance modifications in terms of camouflage, we measured the polarized reflectance from additional incident polarization states to calculate the partial or full Mueller matrices associated with lookdowns, pinfish, and mirrors, and then evaluated the polarization contrast of these targets against the open ocean background for all potential viewing angles.

We calculated a diffuse–reflectance Mueller matrix (19) using these polarized-reflectance measurements wherein each element is an angular average of specular Mueller matrix components with the average taken over a range of angles of incident and reflected illumination (Fig. 2*C*, Table S1). Of note, these measurements are largely independent of illumination and detection numerical aperture, which is consistent with these diffuse–reflectance Mueller matrix elements being largely independent of angle of incidence or reflection (*SI Materials and Methods*) as has been observed for other silvery fish (20). The lookdown measurements indicate a surface that reduces the DoP of incoming 45° polarization with respect to the principle axes, yet preserves the DoP of incident 0° polarization. Although these measurements clearly indicate that lookdowns do not use a vertical mirror reflectance strategy (Fig. 2*C*), does the lookdown strategy provide an increase in polaro–crypsis?

To identify the ideal Mueller matrix properties for polaro–crypsis in an open ocean environment (a Rayleigh scattering field) (21), we model the polarization contrast for reflecting surfaces using an ensemble of possible Mueller matrices assuming the following constraints: (*a*) minimal circular polarization (elliptical elements m_{14}–m_{44} and m_{41}–m_{44} are close to zero), (*b*) minimal dichroic terms (elements m_{12}, m_{13}, m_{21}, and m_{31} are close to zero), (*c*) physical conservation of energy ($\sqrt{m_{22}^2 + m_{32}^2} \leq 1$ and $\sqrt{m_{23}^2 + m_{33}^2} \leq 1$) (22), and (*d*) a flat specular reflecting surface. Conditions *i*, *ii*, and *iv* are consistent with our measurements and

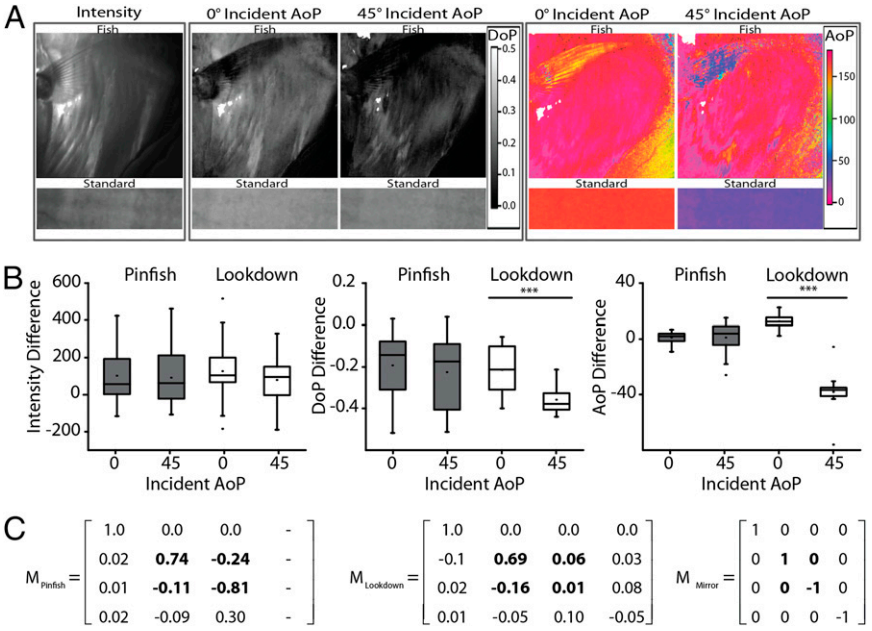

Fig. 2. Polarization reflectance measurements of live fish. (*A*) Video polarimetric images of the intensity, DoP, and AoP of live lookdowns, *S. vomer*, relative to a polarized-reflectance standard composed of silver-screen paint (*Materials and Methods*) under incident illumination conditions simulating high-solar ($\theta_s \sim 90°$, with AoP incident illumination = 0°) and low-solar ($\theta_s \sim 10°$, with AoP incident illumination = 45°) inclination angles with relatively high-incident DoP (0.51 for both 0° and 45° AoP incident illuminations). (*B*) Intensity, DoP, and AoP difference measurements (fish standard) between live restrained lookdowns ($n = 24$ measurements, 4 individuals) and pinfish ($n = 23$ measurements, 8 individuals) relative to a polarized-reflectance standard composed of silver-screen paint (*Materials and Methods*). Box plots display the median and first and third quartiles of measurements, with outliers as points. ***, statistical significance at the $P < 0.001$ level. (*C*) Average Mueller matrices for pinfish and euthanized lookdown measurements along with a Mueller matrix of an idealized vertical mirror.

measurements in the literature (4, 5, 20, 23, 24). These constraints reduce the number of varying Mueller matrix elements to the four central elements (elements m_{22}, m_{32}, m_{23}, and m_{33} in the 4×4 matrix). Polarization contrast, $W = \sqrt{(I_r - I_b)^2 + \frac{1}{2}(Q_r - Q_b)^2 + \frac{1}{2}(U_r - U_b)^2}$, is calculated using a modified form of the rms difference between the reflected and background Stokes vectors, where I, Q, and U are the Stokes vector components corresponding to the reflected and background radiances. Nonnormalized contrasts treat each energy degree-of-freedom in the Stokes radiance values equivalently and, as such, avoid possibly anthropomorphic constructs such as angle or DoP. Further, this type of contrast is directly applicable to physical detection (19). To make these results relevant to polaro–crypsis and ensure the evaluation of the most general strategies possible, numerical averages are taken over the full range of observation angles and fish-body orientation angles (Fig. 3*A*).

Averaging Mueller matrix contrast estimates across all possible viewing angles, we found that the polarized reflectances of mirrors and the nearshore pinfish are both far from the idealized polaro–cryptic strategy in the open ocean environment (Fig. 3*B*). Meanwhile, the lookdown occupies the minimization basin of this polarization-contrast space (Fig. 3*B*, Figs. S1–S3), suggesting that a reflector combined with specific polarization-angle depolarization and polarization-angle modification capability results in optimal crypsis. Lookdowns minimize contrast by having reflectance properties that preserve polarization along the principle axes of the fish and depolarize the polarization along the 45° offset principle axes. This specific feature allows the lookdown to blend in better to the background light at low solar elevations where the background exhibits variable DoP and AoP (Fig. 1). Consider the example of a predator chasing a fish from behind ($\psi = 0°$) and into the sun when the sun is 30° off the horizon (Fig. 1 *E* and *F*), and the fish makes an escape maneuver by veering to the right at a 45° angle ($\varphi = 45°$) (see Fig. 3 for angle definitions). Under these conditions, a pinfish (or mirror-like fish) would likely reflect 45° AoP with high DoP for incident light on its right side, yet the visual background for a pursuant predator is actually what is in front of the fish (0° AoP and low DoP) (Fig. 1 *E* and *F*). Meanwhile, the specific reflectance properties of the lookdown will transform the incident 45° AoP to 0° AoP and also dramatically reduce the reflected DoP. Hence, the specific transforming polarization properties of the lookdown enable it to reduce the contrast against the visual background. Overall, our polaro–crypsis model states that when considering all possible viewing orientations, on average, a predator will see higher polarized reflectance contrast while viewing fish with mirror-like reflectance properties than it will for viewing lookdowns.

The fact that the pinfish from shallow, turbid seas differ significantly from the lookdown indicates that the lookdown polarized reflectance may be a specific adaptation to the constraints of the open ocean. Incorporating the possibility that fish may actively change their body pitch angle (body relative to surface) suggests that lookdowns could potentially gain up to 80% in polaro–crypsis relative to a vertical mirror when considering likely chase angles $|\varphi| < 30°$ (Fig. 4 *A* and *B* and up to 23% polaro–crypsis gain when averaging over all possible observation angles; see also Fig. S4 *A* and *B* and *SI Materials and Methods*). Dynamic modulation and orientational averaging of the polarization properties due to the surface wave field and fluctuations in scattering associated with water property variations result in more complex light fields than those used in our model. Although not completely concealed at all viewing angles, the polaro–cryptic gain that the lookdown surface has over that of a vertical mirror is significant, particularly at low solar inclination angles (Fig. 4 *C* and *D*, Movie S2) and may represent a compromise solution in a complex, dynamic environment. The context-specific angle modification and depolarization features

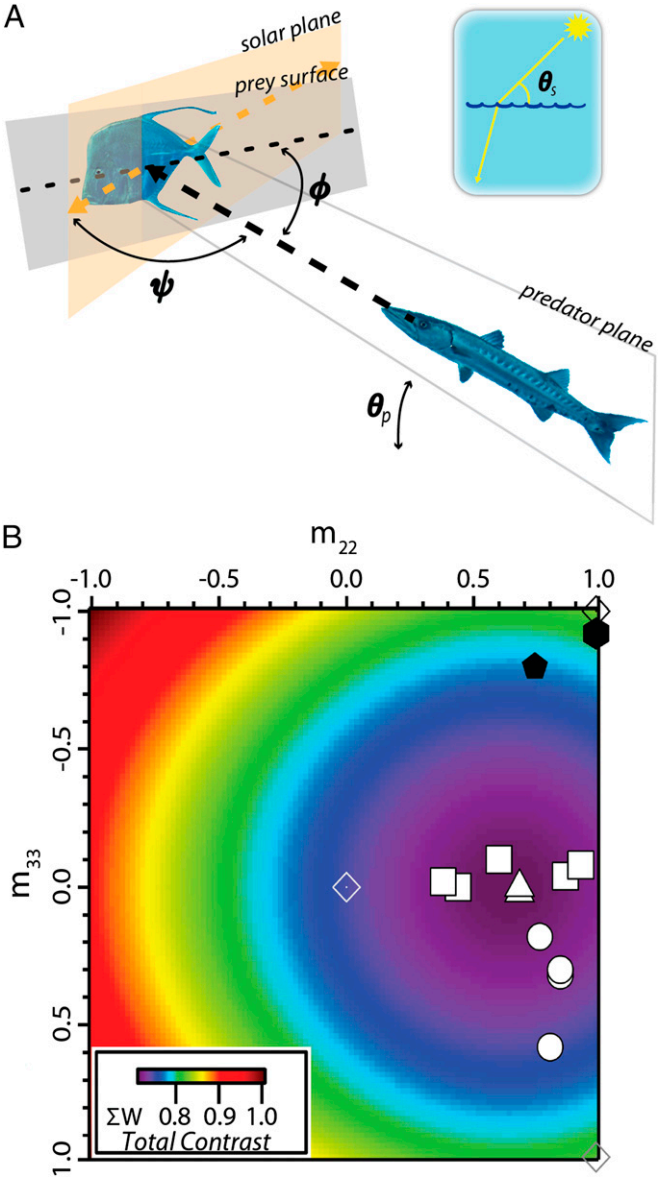

Fig. 3. Modeling polaro–crypsis in the open ocean. (*A*) Four angles parameterize the contrast calculation: θ_s (sun altitude), the inclination angle between the sun and the horizon; θ_p, the inclination angle of the predator from the horizontal; ψ, the azimuthal viewing angle between the predator plane and the solar plane; and φ, the angle between the vertical surface of the prey and the predator (observer) plane. (*B*) The pseudocolor image represents a 2D projection (m_{22} and m_{33} terms only) (for other projections, see Figs. S1–S3) of the summation of the polarization contrast, *W*, over all θ, ψ, and φ angles in 10° increments with $\theta_s = 40°$. The minimum value of the plot (purple) represents the optimal Mueller matrix for polarization crypsis with an unknown predator location. Triangle, circle, and square points are projected locations of the euthanized, microscope-measured, and live lookdowns, respectively, with each point representing an individual fish. The hexagon is the average of the polarization standard measurements, and the pentagon is the average of pinfish measurements. The black, off-white, and gray diamonds represent values for a vertical mirror, a completely depolarizing mirror, and a mirror that acts as a half-wave plate, respectively.

that the lookdown employs as a polaro–crypsis strategy might be engineered by a composite optical structure with a single aligned birefringence axis yet with spatial variation of birefringence magnitude (e.g., a mesh fabricated from thin birefringent film placed over a reflecting surface). It is possible that dynamic control of the lookdown body or skin optical properties (e.g.,

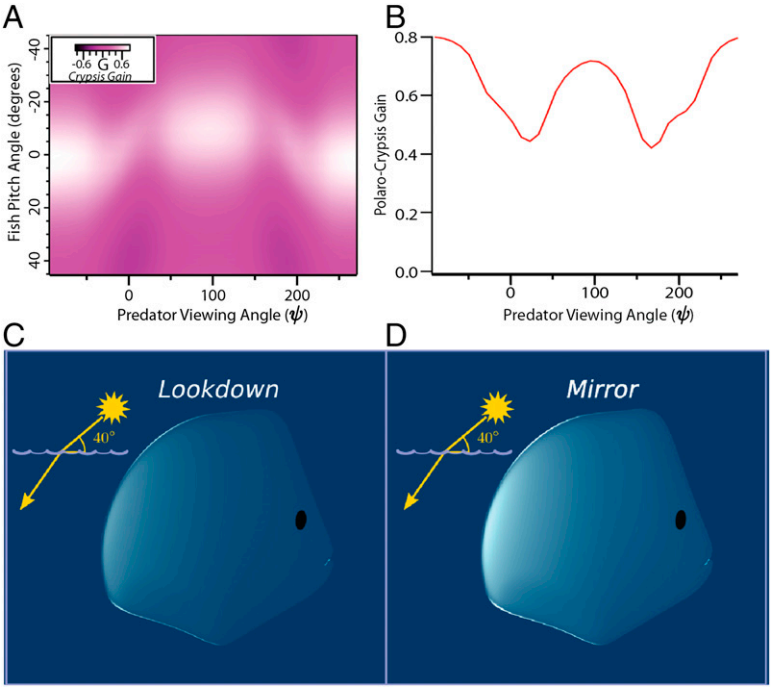

Fig. 4. The Lookdown polaro–crypsis advantage. (*A* and *B*) With $\theta_s = 40°$, the percent crypsis gain is calculated between a vertical mirror (Fig. 2*C*) and the lookdown Mueller matrix (Fig. 2*C*). Figures show the percent gain for (*A*) fish-body pitch angle vs. observation angle summed over a partial angular range of fish-body yaw angles ($|\varphi| < 30°$) and predator inclination angles ($\theta_p = -30°$ to 30°), in 10° increments. White indicates maximal crypsis gain, and pure magenta indicates zero crypsis gain. (*B*) The polaro–crypsis gain (PG) for the optimal fish-body pitch angle from (*A*) calculated as $PG = 100 \times (G_{Lookdown} - G_{verticalmirror})/G_{verticalmirror}$, where *G* is defined as $G = W^{-1}$. The vertical mirror (*C*) is compared with the polaro–cryptic mirror as represented by lookdown measurements (*D*) at the same solar inclination angle (40°). The reflectance used for rendering is calculated as for the analogous panel of Fig. 1 *G* and *H*. Contrast simulations of a reflecting surface with the Mueller matrix elements corresponding to a vertical mirror reveal the vulnerabilities of this strategy to polarization detection when the solar inclination angle deviates from directly overhead (Movie S2).

control of birefringent structures such as guanine platelets and collagen) may additionally improve polaro–crypsis in such dynamic environments. Earlier research has demonstrated that some fish are capable of orientation in polarization-specific directions (25, 26), however no study has yet demonstrated whether fish alter their pitch angle with changes in the polarization environment. Preliminary measurements in our laboratory using neuro-pharmacological manipulation suggest a possible role for dynamic modulation of the lookdown skin optics. Future work examining the dynamic optical properties of lookdown skin as well as determining any associated behavioral strategies, such as control of body orientation, effecting polaro–crypsis of the lookdown in the field will provide insight into the mechanisms of this modulation.

Conclusion

Camouflage strategies must continually evolve as detection capabilities improve. This is true for both biological as well as human endeavors. Polarization-sensitive vision has been demonstrated in many fish and other marine organisms (8–12), implicating a direct selective pressure for the evolution of polarization camouflage. Moreover, manmade polarization-sensitive imaging devices have been shown to double target detection signal-to-noise ratios over conventional imaging technology in scattering media such as the ocean (27, 28). Our findings with the open ocean lookdown and their specific adaptations to maximize polaro–crypsis in the open ocean indicate the likelihood that other fish, as well as human applications requiring such camouflage, may effectively adopt this same strategy.

Materials and Methods

Video Polarimeter. We have constructed a division-of-time video polarimeter capable of recording the complete Stokes vector image (6). This polarimeter employs a standard commercial-grade video camera (Sanyo VPC-FH1ABK), combined with a stack of 2.5 × 5.1 cm^2 liquid crystal π-cells (Liquid Crystal Technologies), which act as electronically controlled birefringent wave plates providing half-wave, quarter-wave, and zero-wave retardation states (29). Dual π-cells with a relative angular offset of 22.5° are combined with a linear polarizer to facilitate the acquisition of the complete Stokes vector (15). In addition, the camera's color Bayer filter provides red, green, and blue (RGB)-channel spectral information. The two π-cells used in this system generate retardation states corresponding to a rotation or angular reflection of the linear polarization of 0°, 45°, 90°, or into a left-circular polarization state.

The video camera itself records 1,080 × 1,920 pixel progressively scanned frames at 60 frames per second. The gamma curves associated with the image sensor are extracted using the algorithm from Robertson et al. (30). We use a custom circuit board based on a MPLABS PIC16F658 microcontroller to synchronize the four π-cell polarization states with the video camera frame timing, and then apply a calibration-generated transformation matrix to convert the intensities of these four video-image frames into the Stokes vector image components. Depending on data analysis requirements, these four image frames may be additionally averaged either temporally (i.e., over multiple sets of four image frames) or spatially. The overall frame rate of the camera is 60 frames per second, with four frames used for data acquisition and two frames used for data buffering. Data processing is performed using custom algorithms implemented in the IGOR-PRO data analysis suite (WaveMetrics).

Polarimeter calibration proceeds using a grid-based approach, in combination with multivariate, least-squares regression. Four hundred and ninety-five known incident polarized-illumination states are established through the use of well-characterized polarization film [PF006, Alight, neutral density (ND) ~ 0.42] and quarter-wave retardation film (560 nm optimal wavelength, WF-OG4, Alight). Individual Mueller matrix elements are estimated using a multivariate least-squares regression between the intensities of consecutive measured video frames and the known incident Stokes vector. These elements are then combined to form the Mueller matrix associating the measured intensity of the four frames to the Stokes components of the incident fields. For intensity calibration of our polarimeter, we used a dense array of fluorescent 5,500 K light bulbs (F15 T8, Full Spectrum) as our incident

illumination in combination with several layers of diffusion filter film and ND filter film (four Rosco 102, two Rosco 114, and a variable number of Lee 209 ND filters). This type of diffusion-filter film reliably provides a uniformly unpolarized light field.

A complete calibration dataset consists of measurements taken over a uniformly distributed set of linear and elliptical polarization angles at 15° increments. In addition, to account for the effects of all relevant physical camera parameters, calibration series are completed for illumination intensity, image-sensor gain, lens focal length, and F-stop. These additional F-stop and focal length calibrations are essential due to the angular dependence of the π-cells. The complete image area is divided into a 35 × 15 grid, and for each grid element, this multivariate regression is completed, resulting in a linear matrix transformation that completely encapsulates the calibration. The multivariate linear regression equation applied is $S_i = M_{ij} I_j$, with M being the matrix of regression parameters, $S = (I, Q, U, V)$, and $I = (I_1, I_2, I_3, I_4)$, where I is the measurement of the four incident intensities. Application of the calibration matrix transformation facilitates the calculation of the Stokes parameters I, Q, U, and V, where I is the total intensity state, Q is the on-axis linear polarization state (0° and 90°), U the 45° off-axis linear polarization state, and V the elliptical or circular polarization state. From the Stokes parameters, we calculate the DoP and the AoP, using the formulas $\mathrm{DoP} = \sqrt{Q^2 + U^2}\,/\mathrm{I}$ and $\mathrm{AoP} = 1/2\ \tan^{-1}(U/Q)$ (19). The ellipticity components were very small in our measurements so they are ignored for simplicity.

Live Fish Measurements. Polarized reflectance measurements were collected from $n = 4$ restrained live lookdown, *S. vomer*, and $n = 8$ restrained live pinfish, *L. rhomboids*, in a white Polyethylene 155 gallon tank under different types of polarized illumination with the imaging polarimeter at the University of Texas Marine Science Institute following our animal care protocol (Institutional Animal Care and Use Committee, protocol AUP-2009-00022) (Fig. S5). The incident illumination setup is designed to allow variation of the incident DoP without altering the illumination intensity by passing light from a 1 kW halogen theatrical lamp (Altman, 75Q, 8-inch Fresnel) through a glass diffusion tank (filled with an aqueous dispersion of magnesium hydroxide particles, a 1:277 dilution of Maalox) and polarization film before entering the experimental tank via a glass porthole. The linear polarizer was placed in different orientations to create incident illumination conditions with discrete AoP properties (0°, 45°, and 90°). The unanesthetized fish were held by hand against a fixed glass partition placed adjacent to a 4 cm × 5 cm polarized-reflectance standard composed of silver-screen paint (Paint On Screen, Inc. S1 Screen Paint Silver) on polystyrene exhibition board backing at 67 cm distance from the illumination source aperture (the 30 cm diameter glass porthole adjacent to the diffusion tank). Polarimetric images of fish were collected with the polarimeter in an underwater housing placed in the same vertical plane as the fish and positioned 26 cm distance away from the fish at a 23° viewing angle (measured with respect to the mean fish-body surface normal). These data were processed into Stokes images using a custom IGOR-PRO data analysis program. Eight regions of interest were selected from the flank of each fish in addition to the polarization reflectance standard.

Euthanized Lookdown Measurements. Polarized reflectance measurements were collected from $n = 2$ freshly euthanized (using clove oil) lookdowns at the University of Texas at Austin to evaluate the Mueller matrix at additional incident-illumination angles. We used a partially collimated incident beam (~0.22 NA) from an ellipsoidal spotlight (Source Four 750 Watt, Electronic Theatre Controls) passing through polarization film (PF006, Alight), quarter-wave retardation film (WF-OG4, Alight), and ND filter film (0.3 ND Lee 209) to illuminate the lookdowns with variable incident AoPs. Fish were restrained horizontally to the back panel and polarimetric images were acquired at 11.25° incident angle increments from 11.25° to 67.5° using the polarimetric imager at a distance of 20 cm.

Anesthetized Lookdown Measurements. Polarized reflectance measurements were collected from $n = 4$ whole juvenile lookdowns freshly anesthetized with clove oil under a microscope outfitted for polarization measurements (Eclipse 80i, Nikon). We collected images of the fish skin at a fixed incoming polarization orientation of 90° with respect to the analyzer, using a 4× objective (0.13 NA) outfitted with a custom antireflecting water-immersion window to reduce the background effect of surface glare on epi-illuminated measurements made in water. Fish bodies were rotated using a rotation stage at 90°,45°,0°, to –45° relative to the head–tail line and the polarization analyzed using a linear polarizer and a quarter-wave plate. Linear polarization was analyzed at 0°, 45°, 90°, 135°, and with an additional quarter-wave plate at the 0° and 90° degree polarization angles. The NA-averaged Mueller matrix was then calculated using these measured values.

ACKNOWLEDGMENTS. We thank Rick Kline for procuring lookdowns, University of Texas Marine Science Institute for facility use, and Ian Etheredge for assistance with graphics. We also thank Kathryn Ruddick and Ian Etheredge for assistance with measurements and data analysis and George Kattawar, Alex Gilerson, Alberto Tonizzo, and Samir Ahmed for advice on the experimental tank design. This research was supported by Office of Naval Research Multidisciplinary University Research Initiative (ONR MURI) Grant N000140911054 (to M.E.C.).

1. Johnsen S (2003) Lifting the cloak of invisibility: The effects of changing optical conditions on pelagic crypsis. *Integr Comp Biol* 43(4):580–590.
2. Marshall NJ, Johnsen S (2011) *Animal Camouflage: Mechanisms and Function*, eds Stevens M, Merilaita S (Cambridge Univ Press, Cambridge, UK), pp 186–211.
3. Denton EJ (1970) Review lecture: On the organization of reflecting surfaces in some marine animals. *Philos Trans R Soc Lond B Biol Sci* 258(824):285–313.
4. Denton EJ, Nicol JAC (1966) A survey of reflectivity in silvery teleosts. *J Mar Biol Assoc UK* 46(3):685–722.
5. Denton EJ, Land MF (1971) Mechanism of reflexion in silvery layers of fish and cephalopods. *Proc R Soc Lond B Biol Sci* 178(50):43–61.
6. You Y, et al. (2011) Measurements and simulations of polarization states of underwater light in clear oceanic waters. *Appl Opt* 50(24):4873–4893.
7. Cronin TW, Shashar N (2001) The linearly polarized light field in clear, tropical marine waters: Spatial and temporal variation of light intensity, degree of polarization and e-vector angle. *Journal of Experimental Biology* 204(14):2461–2467.
8. Shashar N, Hagan R, Boal JG, Hanlon RT (2000) Cuttlefish use polarization sensitivity in predation on silvery fish. *Vision Res* 40(1):71–75.
9. Hawryshyn CW, McFarland WN (1987) Cone photoreceptor mechanisms and the detection of polarized light in fish. *Journal of Comparative Physiology A* 160(4):459–465.
10. Roberts NW, Porter ML, Cronin TW (2011) The molecular basis of mechanisms underlying polarization vision. *Philosophical Transactions of the Royal Society B: Biological Sciences* 366(1565):627–637.
11. Kamermans M, Hawryshyn C (2011) Teleost polarization vision: How it might work and what it might be good for. *Philosophical Transactions of the Royal Society B: Biological Sciences* 366(1565):742–756.
12. Sabbah S, Lerner A, Erlick C, Shashar N (2005) *Recent Research Developments in Experimental & Theoretical Biology*, ed Pandalai SG (Transworld Research Network, Kerala, India), 1:123–176.
13. Waterman TH (2006) Reviving a neglected celestial underwater polarization compass for aquatic animals. *Biol Rev Camb Philos Soc* 81(1):111–115.
14. Waterman TH, Westell WE (1956) Quantitative effects of the sun's position on submarine light polarization. *J Mar Res* 15(2):149–169.
15. Born M, Wolf E (1999) *Principles of Optics: Electromagnetic Theory of Propagation, Interference and Diffraction of Light* (Cambridge Univ Press, Cambridge, UK).
16. Waterman TH (1954) Polarization patterns in submarine illumination. *Science* 120(3127): 927–932.
17. York T, Gruev V (2011) Optical characterization of a polarization imager. *Circuits and Systems (ISCAS), 2011 IEEE International Symposium* 23:1576–1579.
18. Voss KJ, Souaidia N (2010) POLRADS: Polarization radiance distribution measurement system. *Opt Express* 18(19):19672–19680.
19. Goldstein DH (2011) *Polarized Light* (CRC, Boca Raton, FL), 3rd Ed.
20. Jordan TM, Partridge JC, Roberts NW (2012) Non-polarizing broadband multilayer reflectors in fish. *Nature photonics* 6(11):759–763.
21. Sabbah S, Shashar N (2007) Light polarization under water near sunrise. *J Opt Soc Am A Opt Image Sci Vis* 24(7):2049–2056.
22. Fry ES, Kattawar GW (1981) Relationships between elements of the Stokes matrix. *Appl Opt* 20(16):2811–2814.
23. Ivanoff A, Waterman TH (1958) Elliptical polarization of submarine illumination. *J Mar Res* 16(3):255–282.
24. Denton EJ, Nicol JAC (1965) Polarization of light reflected from the silvery exterior of the bleak Alburnus alburnus. *Journal of the Marine Biological Association of the United Kingdom* 45(3):705–709.
25. Hawryshyn CW, Arnold MG, Bowering E, Cole RL (1990) Spatial orientation of rainbow trout to plane-polarized light: The ontogeny of E-vector discrimination and spectral sensitivity characteristics. *Journal of Comparative Physiology A* 166(4):565–574.
26. Groot C (1965) On the orientation of young sockeye salmon (Oncorhynchus nerka), during their seaward migration out of lakes. *Behaviour* 14(1):1–198.
27. Rowe MP, Pugh EN, Jr., Tyo JS, Engheta N (1995) Polarization-difference imaging: A biologically inspired technique for observation through scattering media. *Opt Lett* 20(6):608–610.
28. Tyo JS, Rowe MP, Pugh EN, Jr., Engheta N (1996) Target detection in optically scattering media by polarization-difference imaging. *Appl Opt* 35(11):1855–1870.
29. Bos PJ (1993) *Stereo Computer Graphics and Other True 3D Technologies*, ed McAllister DF (North Carolina State Univ, Raleigh, NC), pp 90–118.
30. Robertson MA, Borman S, Stevenson RL (2003) Estimation-theoretic approach to dynamic range enhancement using multiple exposures. *Journal of Electronic Imaging* 12(2):219–228.